Selenophene–Thiophene Block Copolymer Solar Cells with Thermostable Nanostructures

Dong Gao, Jon Hollinger, and Dwight S. Seferos*

Department of Chemistry, University of Toronto, 80 St. George Street, Toronto, Ontario, M5S 3H6, Canada

ABSTRACT

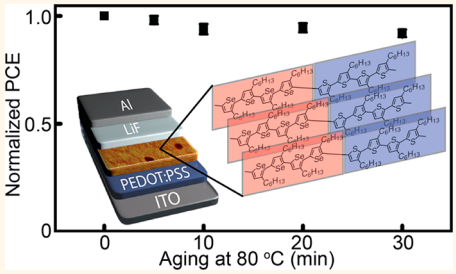

The nanostructure morphology and electron donor performance of a poly(3-hexylselenophene)-*block*-poly(3-hexylthiophene) (P3HS-*b*-P3HT) copolymer was studied in a photovoltaic device with a [6,6]-phenyl C61 butyric acid methyl ester (PCBM) acceptor. P3HS-*b*-P3HT forms fiberlike nanostructures spontaneously, which leads to an initial optimal device performance. Furthermore the nanostructure morphology is not greatly affected by annealing, which leads to a device stability that outperforms P3HT, P3HS, or a P3HS/P3HT mixture under identical conditions. External quantum efficiency, hole mobility, and current–voltage measurements show that the block copolymer also outperforms a ternary blend that consists of a physical mixture of P3HS, P3HT, and PCBM with the same overall composition. Overall, the observation of optimal device performance and morphology without annealing as well as enhanced thermal stability demonstrates the advantage of fully conjugated diblock copolymers in nanostructured devices.

KEYWORDS: conjugated polymer · nanostructure · nanofiber · solar cell · thermal stability

Nanostructured π-conjugated polymers are important chemical compositions that are of interest for a range of optoelectronic uses.[1−3] The structure–property–function relationships in these materials are governed by the molecular arrangement of components. For example, limited by their relatively short exciton diffusion length, which is typically 5–20 nm,[4−7] an optimized donor–acceptor interface network in the bulk-heterojunction (BHJ) system is critical for efficient charge-separation, transport, and hence power conversion efficiency (PCE) of organic photovoltaics (OPVs). Numerous methods have been tested for controlling the nanostructure in OPVs such as thermal annealing,[8−10] vapor annealing,[11−13] or the use of additives.[14−18] Ideal morphologies are achieved though the kinetic control of the crystallization of materials, which varies for different polymer structures and processing conditions. Since the optimal nanoscale morphology may not be the thermodynamically favorable morphology, device deterioration and shorter device lifetimes can be expected as the system ages and converts to a more stable state. Specifically, studies have shown the thermal stability of poly(3-hexylthiophene) (P3HT) or poly[2-methoxy-5-(3′,7′-dimethyloctyloxy)-1,4-phenylenevinylene] (MDMO-PPV) likely limits long-term solar cell performance of these mateirals.[19]

Several researchers have suggested that the challenges with OPV thermal stability could be overcome by decreasing polymer regioregularity[20,21] or using a low molecular weight polymer with a high glass transition temperature.[22] Regioregularity and molecular weight however also affect charge carrier mobility.[23−25] It is therefore difficult to avoid the trade-off between device initial performance and stability. Moreover, annealing is still necessary to reach an initially optimized nanostructure. This latter point is disadvantageous because it adds an additional step and cost to the fabrication process.

Alternatively, thermodynamic phase separation may be achieved through the so-called block copolymer approach. Block copolymers comprise two or more covalently linked polymer blocks with distinct repeat units. One of the most important features of block copolymers is their self-assembly behavior, which provides the possibility to control material domain size or structure at the nanoscale.[26−30] The covalent linkage prevents the two blocks from demixing at the length scale of the polymer chains, typically 10–20 nm, which is roughly equivalent to the exciton diffusion length.[31−42] Our group has

* Address correspondence to dseferos@chem.utoronto.ca.

Received for review May 17, 2012 and accepted June 29, 2012.

Published online July 05, 2012
10.1021/nn3021844

TABLE 1. Summary of Polymer and Device (with PCBM) Characteristics

polymer	M_n[a] kDa	PDI[a]	RR[b] %	HOMO[c] eV	opt. band gap[d] eV	J_{SC} mA cm^{-2}	V_{OC} V	FF %	PCE[e] %	μ_h[f] cm^2 V^{-1} s^{-1}
P3HS-*b*-P3HT	18.3	1.36	85	−5.16	1.60	7.14	0.58	65.05	2.69 (2.52)	2.22×10^{-4}
P3HS/P3HT mixture						6.17	0.58	57.42	2.05 (1.94)	2.88×10^{-5}
P3HT	34.1	1.99	∼95[g]	−5.19	1.90	8.29	0.60	65.94	3.28 (3.12)	5.57×10^{-4}
P3HS	24.1	1.20	83	−5.43	1.61	7.06	0.54	56.11	2.14 (1.85)	4.56×10^{-4}

[a] The number average molecular weight (M_n) and polydispersity index (PDI) from GPC measurements, polystyrene standards were used in the GPC analysis. [b] The regioregularity (RR) determined by NMR. [c] The highest occupied molecular orbital (HOMO) level determined by cyclic voltammetry. [d] The optical band gap determined by the onset of absorption of the polymer film. [e] The average efficiencies of 5−11 devices are inside the brackets. [f] Field-dependent hole mobility (μ_h) measured from single carrier devices. [g] Data was supplied by the manufacturer.

recently introduced poly(3-hexylselenophene)-*block*-poly(3-hexylthiophene) (P3HS-*b*-P3HT), and discovered that blocks of distinct heterocycles undergo a significant degree of phase-separation at the nanoscale.[43,44] On the basis of this observation, we hypothesized that the nanostructure of P3HS-*b*-P3HT will be advantageous for photovoltaic performance. A second unique feature of P3HS-*b*-P3HT copolymers is that each block has a distinct optoelectronic signature and the entire chain is π-conjugated. Blends of multiple donor or acceptor materials, also called ternary blends, are advantageous for controlling device voltage and improving light absorption and current output.[45,46] Therefore, a second hypothesis is that the presence of both the selenophene and thiophene chromophores will provide a better spectral coverage. In this work, we report the first device study of P3HS-*b*-P3HT copolymers and evaluate their performance, nanoscale morphology, and stability as donor materials in OPVs with fullerene acceptors.

RESULTS AND DISCUSSION

The P3HS-*b*-P3HT block copolymers used in this study were synthesized using our previously published procedure.[43] Proton NMR studies were used to confirm the selenophene/thiophene ratio (56:44) by integrating the aromatic resonances, as well as to confirm the block structure. Consistent with our previous work, only selenophene−selenophene and thiophene−thiophene linkages are observed in the NMR spectra of the block copolymer, which rules out any significant monomer mixing (Supporting Information, Figure S6). The regioregularity of the polymer is 85% as determined by NMR. For comparison purposes, the two homopolymers were used as control experiments, as well as a 50:50 physical mixture of each (P3HS/P3HT). We also prepared a 56:44 physical mixture (Supporting Information, Figure S7) and found that the photoresponse was not statistically different from the 50:50 mixture and so we focus on the 50:50 mixture for simplicity. The optical spectra of all the polymers are consistent with previous reports (Supporting Information, Figure S1). The molecular weight of all polymers used in this study are similar (Table 1; Supporting Information, Figure S5). For device fabrication, the active layer is formed by spin-coating a 1:0.8 (w/w) blend of polymer (P3HS-*b*-P3HT, P3HT, P3HS, or P3HS/P3HT) and [6,6]-phenyl C61 butyric acid methyl ester (PCBM) in dichlorobenzene onto an indium tin oxide (ITO) coated glass anode (that was previously coated with a PEDOT/PSS hole transport layer), and finished with a LiF/Al cathode. The active layer thickness is ∼150 nm [determined by atomic force microscopy (AFM)]. The fabrication procedures were optimized separately for each polymer/PCBM device to ensure that in all cases we are comparing the experimentally optimized devices. Accordingly, the P3HT/PCBM active layer was vapor annealed to achieve optimal performance, while the P3HS-*b*-P3HT/PCBM, P3HS/PCBM, and P3HS/P3HT/PCBM active layers were fabricated and dried at 80 °C to achieve optimal performance. A more detailed description of device fabrication can be found in the Methods Section.

The spectral properties and response of the polymer/PCBM photodiodes were studied first. External quantum efficiency (EQE) spectra were measured and compared with the absorption spectra of polymer/PCBM films (Figure 1). Because of the presence of polyselenophene, which has a narrower HOMO−LUMO gap than polythiophene, both P3HS-*b*-P3HT/PCBM and P3HS/P3HT/PCBM films have more red-shifted absorption and EQE response than P3HT/PCBM. The spectra are also broader because they contain two chromophores. The EQE spectrum of P3HS-*b*-P3HT/PCBM shifts to a slightly lower energy (by 0.03 eV) than P3HS. This red shift indicates the block structure has a slightly narrower HOMO−LUMO gap. Interestingly, the EQE in the high energy regions (350−650 nm) are similar for P3HS/PCBM, P3HS-*b*-P3HT/PCBM, and P3HS/P3HT/PCBM films. The photon harvesting in the P3HT-block of P3HS-*b*-P3HT is therefore diminished, as one would ideally expect an intermediate value between P3HT/PCBM and P3HS/PCBM. However, in the region of the EQE spectra where P3HT does not absorb light (650−750 nm), P3HS-*b*-P3HT/PCBM has similar intensity as P3HS/PCBM. In contrast, the response of P3HS/P3HT/PCBM in the same region is roughly half of the intensity of P3HS/PCBM, which is expected because P3HT dilutes the P3HS concentration by about one-half in the film. These results show that the photon harvesting from the P3HS-block is improved in P3HS-*b*-P3HT devices.

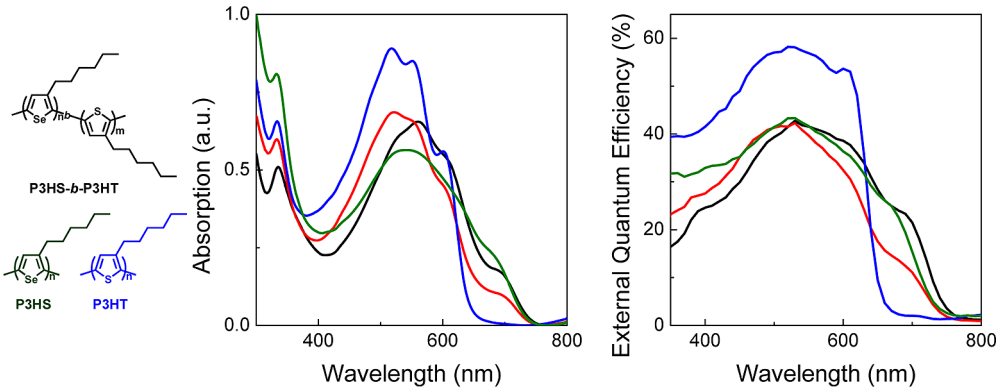

Figure 1. Polymer structures (left), absorption spectra (center), and external quantum efficiency spectra (right) of P3HS-*b*-P3HT/PCBM (black), P3HS/P3HT/PCBM (1:1 mixture of P3HS and P3HT) (red), P3HT/PCBM (blue), and P3HS/PCBM (olive) samples.

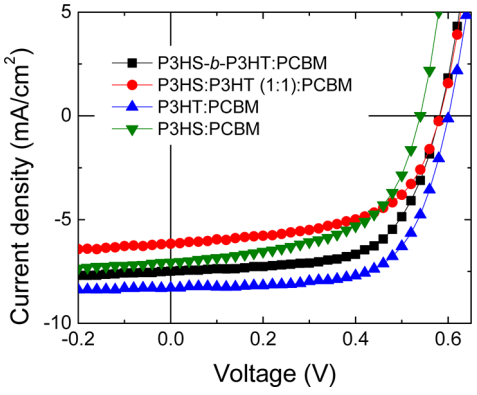

Figure 2. *I*−*V* characteristics of P3HS-*b*-P3HT/PCBM (black), P3HS/P3HT/PCBM 1:1 mixture (red), P3HT/PCBM (blue), and P3HS/PCBM (olive) devices.

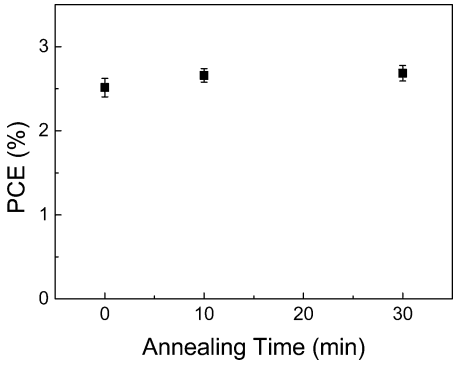

Figure 3. Average power conversion efficiencies of P3HS-*b*-P3HT/PCBM devices annealed at 100 °C as a function of annealing time. Error bars represent the standard deviation of 5−11 devices.

Devices all display typical diode-like *I*−*V* curves under simulated solar illumination (100 mW cm^{-2} AM 1.5 G; Figure 2). The power conversion efficiencies (PCEs) of P3HT/PCBM and P3HS/PCBM devices are consistent with reported literature values.[47−50] P3HS-*b*-P3HT/PCBM and P3HS/P3HT/PCBM devices operate at the same open circuit voltage (V_{oc}) (0.58 V), which is slightly lower than the P3HT/PCBM device (0.60 V) but higher than the P3HS/PCBM device (0.54 V). The V_{oc} is proportional to the difference of the HOMO level of donor and LUMO level of acceptor when the Fermi level is pinned between the organic materials and electrodes.[51] The HOMO levels of P3HT, P3HS, and P3HS-*b*-P3HT are −5.19, −5.43, and −5.16 eV, respectively, as determined by cyclic voltammetry (Supporting Information, Figure S2). The inconsistency between the low-lying HOMO level and low V_{oc} of P3HS/PCBM indicates significant voltage loss, which is likely due to the unfavorable nanomorphology and fast nongeminate recombination of P3HS/PCBM.[48,52] In the P3HS-*b*-P3HT/PCBM system, the presence of P3HT segments appears to improve charge collection from the P3HS segment and results in a higher device V_{oc}. Overall, although the short-circuit current (J_{sc}) of P3HS-*b*-P3HT/PCBM and P3HS/PCBM devices are similar, a higher PCE is achieved in P3HS-*b*-P3HT/PCBM devices owing to a better FF and V_{oc}. We attribute the significantly reduced J_{sc} for P3HS/P3HT/PCBM to the unfavorable morphology of this ternary mixture (*vide infra*).

For homopolymers such as P3HT, thermal or vapor annealing treatment is necessary to achieve optimal device performance.[8] Strikingly, in P3HS-*b*-P3HT/PCBM, the annealed devices are only slightly improved from their initial performance (from 2.5 ± 0.1% without annealing to 2.7 ± 0.1% with annealing; Figure 3). This slight improvement is likely caused by further solvent removal. AFM measurements show that P3HS-*b*-P3HT/PCBM has a nearly identical fiberlike morphology with or without annealing (Figure 4). Although we note that the P3HS-*b*-P3HT/PCBM active layers were spun cast from 80 °C solutions, and dried quickly (~30 s) at these temperatures, this procedure is significantly different than thermal or solvent annealing. This is known as the "fast-grown" process, and a previous study has shown that it will result in a low performance for P3HT/PCBM devices (with PCE lower than 2%).[12] The surface features of the P3HS-*b*-P3HT/PCBM active layer prepared in this manner consist of fibers that are 10−20 nm apart, a distance that is roughly equal to the exciton

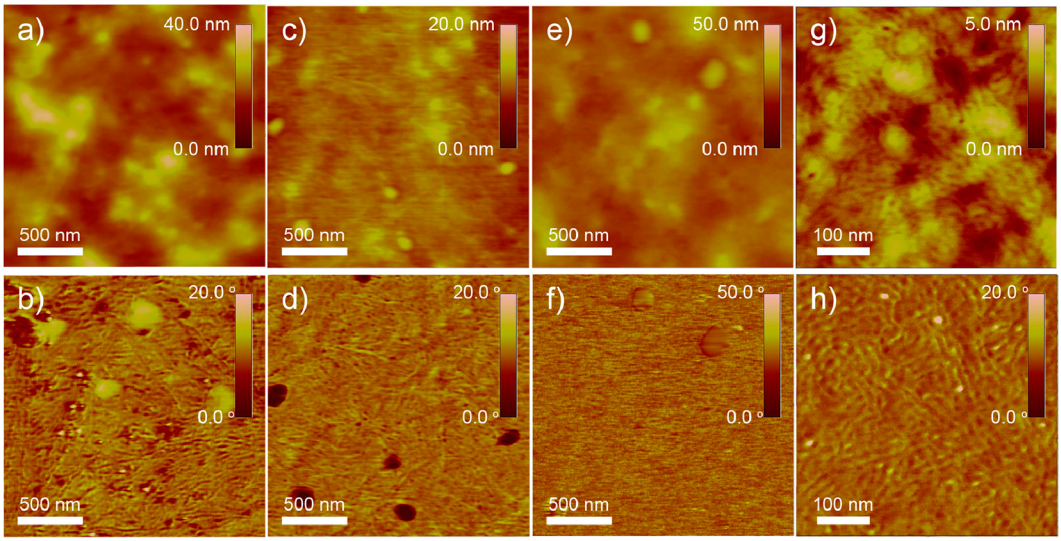

Figure 4. AFM height (a, c, e, g) and phase (b, d, f, h) images of P3HS-*b*-P3HT/PCBM films without annealing (a, b), annealed at 80 °C (c, d), and annealed at 130 °C for 30 min (e, f, g, h).

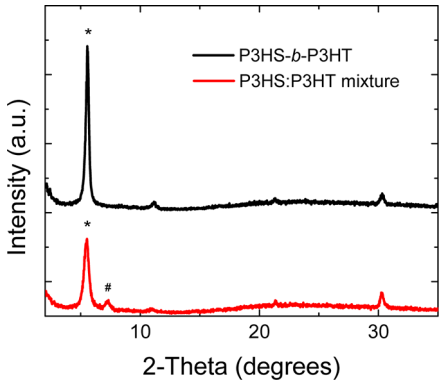

Figure 5. Wide-angle X-ray diffraction patterns (WAXD) of P3HS-*b*-P3HT/PCBM (black) and P3HS/P3HT/PCBM (red) blends drop cast onto ITO/PEDOT/PSS substrates. The peaks at $2\theta \approx 7.3°$ and at $2\theta \approx 5.6°$ correspond to 12.1 Å and 16.0 Å spacing, respectively. The peaks at $2\theta \approx 21.3°$ and 30.2° originate from the ITO substrate.

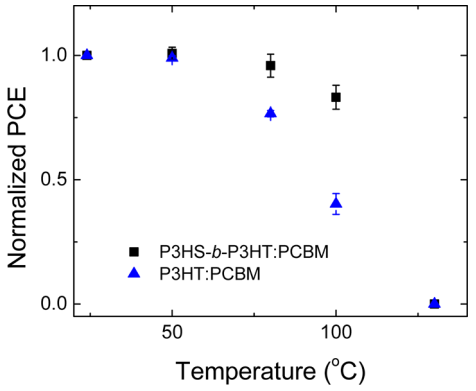

Figure 6. Normalized average PCE as a function of post-annealing temperature of P3HS-*b*-P3HT/PCBM (black) and P3HT/PCBM (blue) devices. The annealing time at each temperature is 10 min. Error bars represent the standard deviation of 5−11 devices.

diffusion length. Fiberlike structures have been observed for nonconjugated polymers that are below the entanglement limit, and for P3HT homopolymers with molecular weights that are below a certain value.[53−55] This structure has been considered to be important to improve phase-separation between the donor and acceptor domains, thereby enhancing charge-transport and separation.[9,31,32,37] This result shows that the fiberlike nanostructure of the P3HS-*b*-P3HT block copolymer film forms spontaneously from solution.

We next designed a series of experiments to further understand the performance of the different polymers in the nanostructured solar cells. The hole mobility of the active layers was determined using the space charge limited current (SCLC) model. In this configuration, P3HT/PCBM has a hole mobility of 5.57×10^{-4} $cm^2V^{-1}s^{-1}$, and P3HS/PCBM has a similar mobility of 4.56×10^{-4} $cm^2V^{-1}s^{-1}$. P3HS-*b*-P3HT/PCBM and P3HT/P3HS/PCBM have hole mobilities of 2.22×10^{-4} $cm^2V^{-1}s^{-1}$ and 2.88×10^{-5} $cm^2V^{-1}s^{-1}$ respectively, which are lower than the values of both P3HT and P3HS. This result indicates that the charge carrier mobility is affected when two distinct polymer domains are present in the hole-conducting material. This could be caused by perturbing the charge-transport process by increasing the energy barrier for charge hopping from one domain to the other. This effect appears minimized in P3HS-*b*-P3HT, likely because it has an organized nanoscale packing arrangement. On the other hand, P3HS/P3HT/PCBM has a very rough and disordered surface (Supporting Information, Figure S3), which is consistent with macroscale demixing, and this likely decreases the overall charge carrier mobility.

In light of this, we examined the differences in the packing arrangements of the polymer in the active layer. Packing arrangement has an important influence on charge carrier mobility and series resistance, which

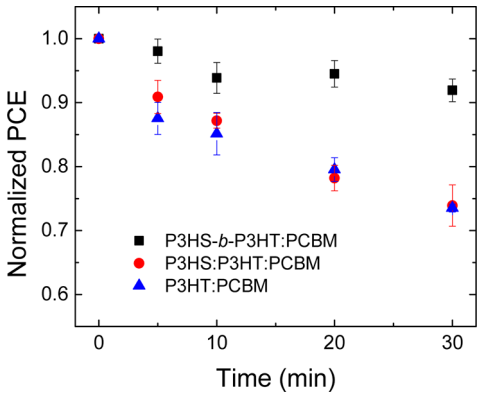

Figure 7. Normalized average PCE as a function of post-annealing time of P3HS-*b*-P3HT/PCBM (black), P3HS/P3HT/PCBM (red), and P3HT/PCBM (blue) devices. The annealing temperature is 80 °C. Error bars represent the standard deviation of 5−11 devices.

can result in a higher J_{sc} and FF.[23] Wide-angle X-ray diffraction patterns (WAXD) of P3HS/P3HT/PCBM blends drop cast onto ITO/PEDOT/PSS substrates reveal peaks at $2\theta \approx 7.3°$ and $2\theta \approx 5.6°$, corresponding to 12.1 Å and 16.0 Å interlayer spacings, respectively (Figure 5). The 12.1 Å spacing has been reported in previous work and is the so-called type-2 polymorph formed by P3HS, which has relatively poor $\pi-\pi$ stacking.[56] In contrast, only a type-1 spacing peak at $2\theta \approx 5.6°$ is observed in the P3HS-*b*-P3HT/PCBM sample indicating that only one polymorph is present in the P3HS-*b*-P3HT film. Because of the similarity in spacing of type-1 P3HT (16.0−16.7 Å)[57,58] and type-1 P3HS (15.2−15.5 Å)[56,59] only one diffraction peak is expected in the P3HS-*b*-P3HT film if both blocks are present in their respective type-1 phases. The presence of two polymorphs in P3HS/P3HT/PCBM may also be indicative of macroscale phase separation, which is consistent with a previous study from our group[44] and the AFM images of this film (Supporting Information, Figure S3). Surface roughness, larger domain sizes, and the presence of two polymorphs of the donor materials in the film are likely the reason why the P3HS/P3HT/PCBM film is less efficient than P3HS-*b*-P3HT/PCBM.

Because annealing does not significantly change the morphology or performance of the P3HS-*b*-P3HT/PCBM device, we hypothesized that one could expect better thermal stability from this system. To investigate thermal stability, we annealed finished devices (hereafter referred to as postannealing) and monitored PCE as a function of both time and temperature. Postannealing and device testing were conducted in a nitrogen-filled glovebox. Impressively, the P3HS-*b*-P3HT/PCBM devices are much more robust to the high temperature postannealing process (Figure 6). After increasing the postannealing temperature to 100 °C, the P3HS-*b*-P3HT/PCBM devices still operate with 83% of their initial efficiencies, while the performance of P3HT/PCBM devices drops by more than

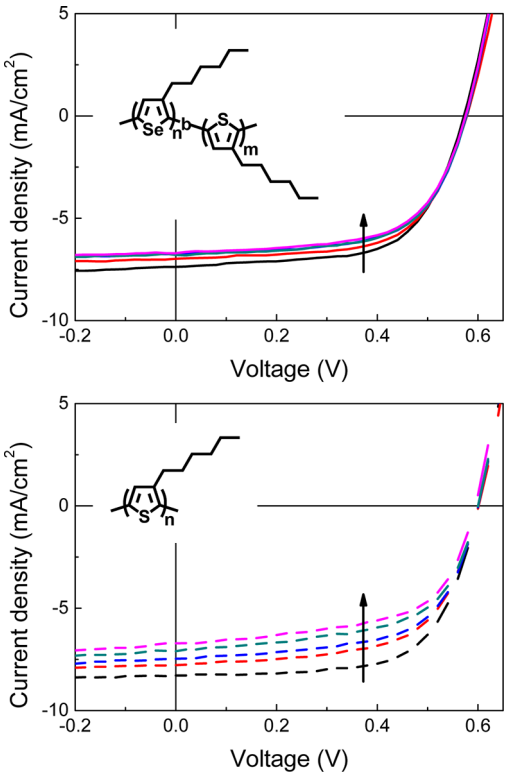

Figure 8. *I*−*V* characteristics of P3HS-*b*-P3HT/PCBM (left) and P3HT/PCBM (right) devices after postannealing at 80 °C for 0 (black), 5 (red), 10 (blue), 20 (olive), and 30 (pink) minutes.

50%. All devices fail (by shorting) after postannealing at 130 °C which may be due to LiF/Al cathode breakdown.

The robustness of P3HS-*b*-P3HT/PCBM devices is also observed during postannealing at fixed temperature as a function of time (Figure 7). P3HT devices lost over 25% PCE after postannealing for 30 min at 80 °C, while P3HS-*b*-P3HT/PCBM devices remain above 90% of the initial operating efficiency under the same experimental conditions. Finally we note that the degradation tendency of the P3HT/P3HS/PCBM mixture is almost identical to P3HT/PCBM, which shows that the block copolymer architecture is necessary for thermal stability. The *I*−*V* curves show that the decline of current is retarded in P3HS-*b*-P3HT/PCBM devices (Figure 8), which is likely due to a stabilized donor−acceptor interface, consistent with AFM measurements. These results demonstrate that a more thermodynamically stable nanostructure is formed by the block copolymer, as devices using P3HS-*b*-P3HT/PCBM are more robust than homopolymers or mixtures.

CONCLUSION

We have studied the morphology of P3HS-*b*-P3HT block copolymers and investigated their photovoltaic performance with a fullerene acceptor for the first time. Fiberlike nanostructures are formed spontaneously in P3HS-*b*-P3HT/PCBM devices, and their thermal stability exceeds homopolymer/PCBM devices or ternary mixtures.

Although P3HS-*b*-P3HT contains two distinct electron donor materials, the EQE spectra, hole mobility, J_{sc}, and PCE exceed that of a physical mixture of the two homopolymers and PCBM. We note further that low energy photoharvesting is improved in this system, relative to either a homopolymer or a physical mixture of both. As ternary and other new OPV systems[7,60−64] are attracting more attention, fully conjugated diblock copolymers should become an important material to study their structure−property−function relationships. These observations should motivate the continued development of other conjugated block copolymers for OPV applications.

METHODS SECTION

General Considerations. All reagents were used as received unless otherwise specified. Selenophene, 2,5-dibromo-3-hexylthiophene, *i*-PrMgCl (2.0 M in THF), and Ni(dppp)Cl_2 [dppp is 1,3-bis(diphenylphosphino)propane] were purchased from Sigma-Aldrich. Solvents were purchased from Caledon Laboratory Chemicals and dried using an Innovative Technology solvent purification system. 2,5-Dibromo-3-hexylselenophene was synthesized from selenophene as previously reported.[43] P3HT was purchased from Rieke Metals Inc. [6,6]-Phenyl C61 butyric acid methyl ester (PCBM) was purchased from Nano C Inc. NMR spectra were recorded on a Varian Mercury 400 spectrometer operating at 400 MHz. Chemical shifts are reported in ppm at ambient temperature. ^{1}H chemical shifts are referenced to the residual protonated chloroform peak at 7.26 ppm. Polymer molecular weights were determined with a Viscotek HT-GPC (1,2,4-trichlorobenzene, 140 °C, 1 mL/min flow rate) using Tosoh Bioscience LLC TSK-GEL GMHHR-HT mixed-bed columns and narrow molecular weight distribution polystyrene standards. A UV−vis (450 nm) detector was used to detect the eluted polymer with respect to elution volume. Absorption spectra were recorded on a Varian Cary 5000 UV−vis−NIR spectrophotometer. Electrochemistry was performed with a BASi Epsilon potentiostat. AFM images were obtained with a Vecco Dimension 3000 microscope. Powder X-ray diffraction spectra were recorded on a Bruker AXS D8 Discovery with a GADDS area detector. *I*−*V* characteristics were measured using a Keithley 2400 source meter under simulated AM 1.5 G conditions with a power intensity of 100 mW/cm^2. The mismatch of simulator spectrum was calibrated using a Si diode with a KG-5 filter. EQE spectra were measured using a 300 W xenon lamp with an Oriel Cornerstone 260 1/4 m monochromator and compared with a Si reference cell that is traceable to the National Institute of Standards and Technology.

Polymer Synthesis. *(Poly-3-hexylselenophene)-block-(poly-3-hexylthiophene) (P3HS-b-P3HT).* A Schlenk flask was loaded with 2,5-dibromo-3-hexylselenophene (1.09 g, 2.92 mmol) and evacuated for 20 min. THF (22 mL) was then added followed by *i*-PrMgCl (1.46 mL, 2.0 M in THF). After 1 h the mixture was transferred to a flask containing Ni(dppp)Cl_2 (31 mg, 0.057 mmol) for polymerization and heated to 40 °C for 20 min. In a separate flask, 2,5-dibromo-3-hexylthiophene (0.95 g, 2.92 mmol) was treated with THF (22 mL) and *i*-PrMgCl (1.46 mL) and stirred for 1 h at room temperature. The thiophene monomer solution was transferred to the polymerization flask after the selenophene monomer had polymerized for 20 min. The reaction was continued for another 20 min and then quenched with 5% HCl, precipitated in methanol, filtered, and dried to afford a dark purple solid (750 mg, 68%). For polymer device testing, a fraction of this material was purified by Soxhlet extraction in methanol, hexanes, and chloroform. The chloroform fraction was passed through a silica plug eluting with chloroform, and the solvent was removed under vacuum. The selenophene/thiophene ratio (56:44) was determined by integrating the aromatic peaks from the two distinct heterocycles (7.12 ppm and 6.98 ppm for selenophene and thiophene, respectively). ^{1}H NMR ($CDCl_3$, 300 MHz): δ 7.12 (s), 6.98 (s), 2.80 (t), 2.73 (t), 1.69 (m), 1.43, (m), 1.35 (m), 0.91 (m), 85% regioregular; GPC (140 °C in 1,2,4-tricholorobenzene): M_n = 18.3 kDa, M_w = 25.0 kDa, PDI = 1.36.

Poly-3-hexylselenophene (P3HS). A Schlenk flask was loaded with 2,5-dibromo-3-hexylselenophene (1.01 g, 2.71 mmol) and evacuated for 20 min. THF (19 mL) was then added followed by *i*-PrMgCl (1.35 mL, 2.0 M in THF). After 1 h the mixture was transferred to a flask containing Ni(dppp)Cl_2 (14.6 mg, 0.027 mmol) for polymerization. The mixture was heated to 40 °C for 20 min and then quenched with 5% HCl. The polymer was then precipitated into methanol and filtered to afford a purple solid (314 mg, 54% yield). For device testing, this material was placed in a Soxhlet thimble and extracted with methanol, hexanes, and chloroform. The chloroform fraction was passed through a plug of silica eluting with chloroform and the solvent was removed under vacuum. ^{1}H NMR ($CDCl_3$, 300 MHz): δ 7.12 (s), 2.73 (t), 1.67 (m), 1.43 (m). 1.34 (m), 0.90 (t), 83% regioregular; GPC (140 °C in 1,2,4-tricholorobenzene): M_n = 24.1 kDa, M_w = 28.6 kDa, PDI = 1.20.

Device Fabrication. P3HT, P3HS, or P3HS-*b*-P3HT and PCBM were mixed in 1,2-dichlorobenzene (15 mg/mL total polymer: 12 mg/mL PCBM) and stirred for 16 h at 80 °C to completely dissolve the solids. Devices were fabricated on commercial indium tin oxide (ITO) substrates (Colorado Concept Coatings) that had a sheet resistance of ∼10 Ω/□. These substrates were cleaned in aqueous detergent, deionized (DI) water, acetone, and methanol, and subsequently treated in an oxygen-plasma cleaner for 5 min. Next, poly(3,4-ethylenedioxythiophene)/poly(styrenesulfonate) (PEDOT/PSS) (Clevios P VP AI 4083) was coated onto the substrates at 3000 rpm and the PEDOT/PSS-coated substrates were annealed in air at 130 °C for 15 min. After annealing, the substrates were transferred into a nitrogen-filled glovebox, where polymer/PCBM blends were coated at 800 rpm. After spin-coating, P3HT samples were immediately transferred into closed Petri-dishes and slowly dried at room temperature (a vapor annealing process; the optimized condition). For P3HS, P3HS-*b*-P3HT, and P3HS/P3HT samples, films were spin-coated from hot solutions followed by heating at 80 °C until the films were dry (determined by the color change from solution to film, ∼30 s). This annealing treatment was carried out on a hot plate in glovebox before transferring the samples into an evaporation chamber. A 0.8 nm LiF layer and 100 nm Al anode was thermally deposited through a shadow mask at ∼10^{-6} Torr. The device area is 0.07 cm^2 as defined by the area of circular Al anode. Postannealing was carried out after depositing this top electrode. *I*−*V* characteristics were measured under simulated AM 1.5 G conditions with a power intensity of 100 mW/cm^2. The averages and standard deviations are calculated from 5−11 individual devices. The thickness of active layer is ∼150 nm for all devices, determined by AFM. Single carrier devices were fabricated in the same manner as photodiode devices except the LiF/Al cathode was replaced by a Au cathode. *I*−*V* characteristics of the single carrier devices were measured under dark conditions and mobility was estimated from the Mott−Gurney law (Supporting Information, Figure S4).

Conflict of Interest: The authors declare no competing financial interest.

Supporting Information Available: Additional characterization and device data. This material is available free of charge *via* the Internet at http://pubs.acs.org.

Acknowledgment. The authors thank Dr. Srebri Petrov for WAXD measurements and Dr. Weiqing Shi for assistance with AFM imaging. This work was supported by the University of

Toronto, NSERC, the CFI, and the Ontario Research Fund. D.S.S. is grateful to the Ontario Research Fund (for an Early Researcher Award), MaRS Innovation (for a Proof-of-Principle Grant), the Connaught Foundation (for an Innovation Award), and DuPont Central Research (for a Young Professor Grant) for support of this work.

REFERENCES AND NOTES

1. Yu, G.; Gao, J.; Hummelen, J. C.; Wudl, F.; Heeger, A. J. Polymer Photovoltatic Cells—Enhanced Efficiencies *via* a Network of Internal Donor−Acceptor Heterojunctions. *Science* **1995**, *270*, 1789–1791.
2. Burroughes, J. H.; Bradley, D. D. C.; Brown, A. R.; Marks, R. N.; Mackay, K.; Friend, R. H.; Burns, P. L.; Holmes, A. B. Light-Emitting-Diodes Based on Conjugatd Polymers. *Nature* **1990**, *347*, 539–541.
3. Adronov, A.; Gilat, S. L.; Frechet, J. M. J.; Ohta, K.; Neuwahl, F. V. R.; Fleming, G. R. Light Harvesting and Energy Transfer in Laser-Dye-Labeled Poly(aryl ether) Dendrimers. *J. Am. Chem. Soc.* **2000**, *122*, 1175–1185.
4. Blom, P. W. M.; Mihailetchi, V. D.; Koster, L. J. A.; Markov, D. E. Device Physics of Polymer: Fullerene Bulk Heterojunction Solar Cells. *Adv. Mater.* **2007**, *19*, 1551–1566.
5. Thompson, B. C.; Frechet, J. M. J. Organic Photovoltaics—Polymer−Fullerene Composite Solar Cells. *Angew. Chem., Int. Ed.* **2008**, *47*, 58–77.
6. Yang, F.; Forrest, S. R. Photocurrent Generation in Nanostructured Organic Solar Cells. *ACS Nano* **2008**, *2*, 1022–1032.
7. Yan, H.; Collins, B. A.; Gann, E.; Wang, C.; Ade, H.; McNeill, C. R. Correlating the Efficiency and Nanomorphology of Polymer Blend Solar Cells Utilizing Resonant Soft X-ray Scattering. *ACS Nano* **2011**, *6*, 677–688.
8. Ma, W. L.; Yang, C. Y.; Gong, X.; Lee, K.; Heeger, A. J. Thermally Stable, Efficient Polymer Solar Cells with Nanoscale Control of the Interpenetrating Network Morphology. *Adv. Funct. Mater.* **2005**, *15*, 1617–1622.
9. Yang, X. N.; Loos, J.; Veenstra, S. C.; Verhees, W. J. H.; Wienk, M. M.; Kroon, J. M.; Michels, M. A. J.; Janssen, R. A. J. Nanoscale Morphology of High-Performance Polymer Solar Cells. *Nano Lett.* **2005**, *5*, 579–583.
10. Padinger, F.; Rittberger, R. S.; Sariciftci, N. S. Effects of Postproduction Treatment on Plastic Solar Cells. *Adv. Funct. Mater.* **2003**, *13*, 85–88.
11. Chang, L.; Lademann, H. W. A.; Bonekamp, J.-B.; Meerholz, K.; Moule, A. J. Effect of Trace Solvent on the Morphology of P3HT/PCBM Bulk Heterojunction Solar Cells. *Adv. Funct. Mater.* **2011**, *21*, 1779–1787.
12. Li, G.; Shrotriya, V.; Huang, J. S.; Yao, Y.; Moriarty, T.; Emery, K.; Yang, Y. High-Efficiency Solution Processable Polymer Photovoltaic Cells by Self-Organization of Polymer Blends. *Nat. Mater.* **2005**, *4*, 864–868.
13. Zhao, Y.; Xie, Z.; Qu, Y.; Geng, Y.; Wang, L. Solvent-Vapor Treatment Induced Performance Enhancement of Poly(3-hexylthiophene): Methanofullerene Bulk-Heterojunction Photovoltaic Cells. *Appl. Phys. Lett.* **2007**, *90*, 043504.
14. Hoven, C. V.; Dang, X. D.; Coffin, R. C.; Peet, J.; Nguyen, T. Q.; Bazan, G. C. Improved Performance of Polymer Bulk Heterojunction Solar Cells through the Reduction of Phase Separation *via* Solvent Additives. *Adv. Mater.* **2010**, *22*, E63–E66.
15. Peet, J.; Kim, J. Y.; Coates, N. E.; Ma, W. L.; Moses, D.; Heeger, A. J.; Bazan, G. C. Efficiency Enhancement in Low-Bandgap Polymer Solar Cells by Processing with Alkane Dithiols. *Nat. Mater.* **2007**, *6*, 497–500.
16. Lee, J. K.; Ma, W. L.; Brabec, C. J.; Yuen, J.; Moon, J. S.; Kim, J. Y.; Lee, K.; Bazan, G. C.; Heeger, A. J. Processing Additives for Improved Efficiency from Bulk Heterojunction Solar Cells. *J. Am. Chem. Soc.* **2008**, *130*, 3619–3623.
17. Liu, X. L.; Huettner, S.; Rong, Z. X.; Sommer, M.; Friend, R. H. Solvent Additive Control of Morphology and Crystallization in Semiconducting Polymer Blends. *Adv. Mater.* **2012**, *24*, 669–674.
18. Lobez, J. M.; Andrew, T. L.; Bulović, V.; Swager, T. M. Improving the Performance of P3HT−Fullerene Solar Cells with Side-Chain-Functionalized Poly(thiophene) Additives: A New Paradigm for Polymer Design. *ACS Nano* **2012**, *6*, 3044–3056.
19. Jorgensen, M.; Norrman, K.; Krebs, F. C. Stability/Degradation of Polymer Solar Cells. *Sol. Energy Mater. Sol. Cells* **2008**, *92*, 686–714.
20. Woo, C. H.; Thompson, B. C.; Kim, B. J.; Toney, M. F.; Frechet, J. M. J. The Influence of Poly(3-hexylthiophene) Regioregularity on Fullerene-Composite Solar Cell Performance. *J. Am. Chem. Soc.* **2008**, *130*, 16324–16329.
21. Sivula, K.; Luscombe, C. K.; Thompson, B. C.; Frechet, J. M. J. Enhancing the Thermal Stability of Polythiophene: Fullerene Solar Cells by Decreasing Effective Polymer Regioregularity. *J. Am. Chem. Soc.* **2006**, *128*, 13988–13989.
22. Ebadian, S.; Gholamkhass, B.; Shambayati, S.; Holdcroft, S.; Servati, P. Effects of Annealing and Degradation on Regioregular Polythiophene-Based Bulk Heterojunction Organic Photovoltaic Devices. *Sol. Energy Mater. Sol. Cells* **2010**, *94*, 2258–2264.
23. Kim, Y.; Cook, S.; Tuladhar, S. M.; Choulis, S. A.; Nelson, J.; Durrant, J. R.; Bradley, D. D. C.; Giles, M.; McCulloch, I.; Ha, C. S.; *et al*. A Strong Regioregularity Effect in Self-Organizing Conjugated Polymer Films and High-Efficiency Polythiophene: Fullerene Solar Cells. *Nat. Mater.* **2006**, *5*, 197–203.
24. Zen, A.; Saphiannikova, M.; Neher, D.; Grenzer, J.; Grigorian, S.; Pietsch, U.; Asawapirom, U.; Janietz, S.; Scherf, U.; Lieberwirth, I.; *et al*. Effect of Molecular Weight on the Structure and Crystallinity of Poly(3-hexylthiophene). *Macromolecules* **2006**, *39*, 2162–2171.
25. Reid, O. G.; Malik, J. A. N.; Latini, G.; Dayal, S.; Kopidakis, N.; Silva, C.; Stingelin, N.; Rumbles, G. The Influence of Solid-State Microstructure on the Origin and Yield of Long-Lived Photogenerated Charge in Neat Semiconducting Polymers. *J. Polym. Sci., Part B: Polym. Phys.* **2012**, *50*, 27–37.
26. Chai, J.; Buriak, J. M. Using Cylindrical Domains of Block Copolymers To Self-Assemble and Align Metallic Nanowires. *ACS Nano* **2008**, *2*, 489–501.
27. Wu, N. L. Y.; Zhang, X.; Murphy, J. N.; Chai, J.; Harris, K. D.; Buriak, J. M. Density Doubling of Block Copolymer Templated Features. *Nano Lett.* **2011**, *12*, 264–268.
28. Watson, K. J.; Zhu, J.; Nguyen, S. T.; Mirkin, C. A. Hybrid Nanoparticles with Block Copolymer Shell Structures. *J. Am. Chem. Soc.* **1998**, *121*, 462–463.
29. Forrey, C.; Yager, K. G.; Broadaway, S. P. Molecular Dynamics Study of the Role of the Free Surface on Block Copolymer Thin Film Morphology and Alignment. *ACS Nano* **2011**, *5*, 2895–2907.
30. Wu, Z.-Q.; Ono, R. J.; Chen, Z.; Bielawski, C. W. Synthesis of Poly(3-alkylthiophene)-block-poly(arylisocyanide): Two Sequential, Mechanistically Distinct Polymerizations Using a Single Catalyst. *J. Am. Chem. Soc.* **2010**, *132*, 14000–14001.
31. Zhang, Y.; Tajima, K.; Hirota, K.; Hashimoto, K. Synthesis of All-Conjugated Diblock Copolymers by Quasi-Living Polymerization and Observation of Their Microphase Separation. *J. Am. Chem. Soc.* **2008**, *130*, 7812–7813.
32. Ren, G.; Wu, P.-T.; Jenekhe, S. A. Solar Cells Based on Block Copolymer Semiconductor Nanowires: Effects of Nanowire Aspect Ratio. *ACS Nano* **2011**, *5*, 376–384.
33. Griffini, G.; Douglas, J. D.; Piliego, C.; Holcombe, T. W.; Turri, S.; Frechet, J. M. J.; Mynar, J. L. Long-Term Thermal Stability of High-Efficiency Polymer Solar Cells Based on Photocrosslinkable Donor−Acceptor Conjugated Polymers. *Adv. Mater.* **2011**, *23*, 1660–1664.
34. Zhou, Z.; Chen, X.; Holdcroft, S. Stabilizing Bicontinuous Nanophase Segregation in Pi CP-C(60) Donor−Acceptor Blends. *J. Am. Chem. Soc.* **2008**, *130*, 11711–11718.
35. Zhang, Q. L.; Cirpan, A.; Russell, T. P.; Emrick, T. Donor−Acceptor Poly(thiophene-block-perylene diimide) Copolymers: Synthesis and Solar Cell Fabrication. *Macromolecules* **2009**, *42*, 1079–1082.
36. Mulherin, R. C.; Jung, S.; Huettner, S.; Johnson, K.; Kohn, P.; Sommer, M.; Allard, S.; Scherf, U.; Greenham, N. C. Ternary Photovoltaic Blends Incorporating an All-Conjugated

Donor–Acceptor Diblock Copolymer. *Nano Lett.* **2011**, *11*, 4846–4851.
37. Sun, Z.; Xiao, K.; Keum, J. K.; Yu, X.; Hong, K.; Browning, J.; Ivanov, I. N.; Chen, J.; Alonzo, J.; Li, D.; *et al*. PS-b-P3HT Copolymers as P3HT/PCBM Interfacial Compatibilizers for High Efficiency Photovoltaics. *Adv. Mater.* **2011**, *23*, 5529–5535.
38. Botiz, I.; Schaller, R. D.; Verduzco, R.; Darling, S. B. Optoelectronic Properties and Charge Transfer in Donor–Acceptor All-Conjugated Diblock Copolymers. *J. Phys. Chem. C* **2011**, *115*, 9260–9266.
39. Sommer, M.; Lindner, S. M.; Thelakkat, M. Microphase-Separated Donor–Acceptor Diblock Copolymers: Influence of HOMO Energy Levels and Morphology on Polymer Solar Cells. *Adv. Funct. Mater.* **2007**, *17*, 1493–1500.
40. Sommer, M.; Huttner, S.; Steiner, U.; Thelakkat, M. Influence of Molecular Weight on the Solar Cell Performance of Double-Crystalline Donor–Acceptor Block Copolymers. *Appl. Phys. Lett.* **2009**, *95*, 183308.
41. Yang, C.; Lee, J. K.; Heeger, A. J.; Wudl, F. Well-Defined Donor–Acceptor Rod-Coil Diblock Copolymers Based on P3HT Containing C(60): The Morphology and Role as a Surfactant in Bulk-Heterojunction Solar Cells. *J. Mater. Chem.* **2009**, *19*, 5416–5423.
42. Sary, N.; Richard, F.; Brochon, C.; Leclerc, N.; Leveque, P.; Audinot, J. N.; Berson, S.; Heiser, T.; Hadziioannou, G.; Mezzenga, R. A New Supramolecular Route for Using Rod–Coil Block Copolymers in Photovoltaic Applications. *Adv. Mater.* **2010**, *22*, 763–768.
43. Hollinger, J.; Jahnke, A. A.; Coombs, N.; Seferos, D. S. Controlling Phase Separation and Optical Properties in Conjugated Polymers through Selenophene–Thiophene Copolymerization. *J. Am. Chem. Soc.* **2010**, *132*, 8546–8547.
44. Hollinger, J.; DiCarmine, P. M.; Karl, D.; Seferos, D. S. Heterocycle-Induced Phase Separation in Conjugated Polymers. *Macromolecules* **2012**, *45*, 3772–3778.
45. Khlyabich, P. P.; Burkhart, B.; Thompson, B. C. Efficient Ternary Blend Bulk Heterojunction Solar Cells with Tunable Open-Circuit Voltage. *J. Am. Chem. Soc.* **2011**, *133*, 14534–14537.
46. Yang, L.; Zhou, H.; Price, S. C.; You, W. Parallel-like Bulk Heterojunction Polymer Solar Cells. *J. Am. Chem. Soc.* **2012**, *134*, 5432–5435.
47. Dang, M. T.; Hirsch, L.; Wantz, G. P3HT/PCBM, Best Seller in Polymer Photovoltaic Research. *Adv. Mater.* **2011**, *23*, 3597–3602.
48. Maurano, A.; Shuttle, C. C.; Hamilton, R.; Ballantyne, A. M.; Nelson, J.; Zhang, W.; Heeney, M.; Durrant, J. R. Transient Optoelectronic Analysis of Charge Carrier Losses in a Selenophene/Fullerene Blend Solar Cell. *J. Phys. Chem. C* **2011**, *115*, 5947–5957.
49. Ballantyne, A. M.; Chen, L. C.; Nelson, J.; Bradley, D. D. C.; Astuti, Y.; Maurano, A.; Shuttle, C. G.; Durrant, J. R.; Heeney, M.; Duffy, W.; *et al*. Studies of Highly Regioregular Poly(3-hexylselenophene) for Photovoltaic Applications. *Adv. Mater.* **2007**, *19*, 4544–4547.
50. Gao, D.; Seferos, D. S. Size-Dependent Behavior of Polymer Solar Cells Measured under Partial Illumination. *Solar Sol. Energy Mater. Sol. Cells* **2011**, *95*, 3516–3519.
51. Brabec, C. J.; Cravino, A.; Meissner, D.; Sariciftci, N. S.; Fromherz, T.; Rispens, M. T.; Sanchez, L.; Hummelen, J. C. Origin of the Open Circuit Voltage of Plastic Solar Cells. *Adv. Funct. Mater.* **2001**, *11*, 374–380.
52. Maurano, A.; Hamilton, R.; Shuttle, C. G.; Ballantyne, A. M.; Nelson, J.; O'Regan, B.; Zhang, W. M.; McCulloch, I.; Azimi, H.; Morana, M.; *et al*. Recombination Dynamics as a Key Determinant of Open Circuit Voltage in Organic Bulk Heterojunction Solar Cells: A Comparison of Four Different Donor Polymers. *Adv. Mater.* **2010**, *22*, 4987–4992.
53. Kline, R. J.; McGehee, M. D.; Kadnikova, E. N.; Liu, J.; Fréchet, J. M. J.; Toney, M. F. Dependence of Regioregular Poly(3-hexylthiophene) Film Morphology and Field-Effect Mobility on Molecular Weight. *Macromolecules* **2005**, *38*, 3312–3319.
54. Zhang, R.; Li, B.; Iovu, M. C.; Jeffries-El, M.; Sauvé, G.; Cooper, J.; Jia, S.; Tristram-Nagle, S.; Smilgies, D. M.; Lambeth, D. N.; *et al*. Nanostructure Dependence of Field-Effect Mobility in Regioregular Poly(3-hexylthiophene) Thin Film Field Effect Transistors. *J. Am. Chem. Soc.* **2006**, *128*, 3480–3481.
55. Brinkmann, M.; Rannou, P. Effect of Molecular Weight on the Structure and Morphology of Oriented Thin Films of Regioregular Poly(3-hexylthiophene) Grown by Directional Epitaxial Solidification. *Adv. Funct. Mater.* **2007**, *17*, 101–108.
56. Li, L.; Hollinger, J.; Jahnke, A. A.; Petrov, S.; Seferos, D. S. Polyselenophenes with Distinct Crystallization Properties. *Chem. Sci.* **2011**, *2*, 2306–2310.
57. McCullough, R. D.; Tristramnagle, S.; Williams, S. P.; Lowe, R. D.; Jayaraman, M. Self-Orienting Head-to-Tail Poly(3-alkylthiophenes)—New Insights on Structure–Property Relationship in Conducting Polymers. *J. Am. Chem. Soc.* **1993**, *115*, 4910–4911.
58. Wu, P. T.; Ren, G. Q.; Kim, F. S.; Li, C. X.; Mezzenga, R.; Jenekhe, S. A. Poly(3-hexylthiophene)-*b*-poly(3-cyclohexylthiophene): Synthesis, Microphase Separation, Thin Film Transistors, and Photovoltaic Applications. *J. Polym. Sci., Part A: Polym. Chem.* **2010**, *48*, 614–626.
59. Heeney, M.; Zhang, W.; Crouch, D. J.; Chabinyc, M. L.; Gordeyev, S.; Hamilton, R.; Higgins, S. J.; McCulloch, I.; Skabara, P. J.; Sparrowe, D.; *et al*. Regioregular Poly(3-hexyl) Selenophene: A Low Band Gap Organic Hole Transporting Polymer. *Chem. Commun.* **2007**, *47*, 5061–5063.
60. Schierhorn, M.; Boettcher, S. W.; Peet, J. H.; Matioli, E.; Bazan, G. C.; Stucky, G. D.; Moskovits, M. CdSe Nanorods Dominate Photocurrent of Hybrid CdSe–P3HT Photovoltaic Cell. *ACS Nano* **2010**, *4*, 6132–6136.
61. Kamkar, D. A.; Wang, M.; Wudl, F.; Nguyen, T.-Q. Single Nanowire OPV Properties of a Fullerene-Capped P3HT Dyad Investigated Using Conductive and Photoconductive AFM. *ACS Nano* **2012**, *6*, 1149–1157.
62. Rice, A. H.; Giridharagopal, R.; Zheng, S. X.; Ohuchi, F. S.; Ginger, D. S.; Luscombe, C. K. Controlling Vertical Morphology within the Active Layer of Organic Photovoltaics Using Poly(3-hexylthiophene) Nanowires and Phenyl-C61-butyric Acid Methyl Ester. *ACS Nano* **2011**, *5*, 3132–3140.
63. Tevis, I. D.; Tsai, W.-W.; Palmer, L. C.; Aytun, T.; Stupp, S. I. Grooved Nanowires from Self-Assembling Hairpin Molecules for Solar Cells. *ACS Nano* **2012**, *6*, 2032–2040.
64. Ferenczi, T. A. M.; Mueller, C.; Bradley, D. D. C.; Smith, P.; Nelson, J.; Stingelin, N. Organic Semiconductor: Insulator Polymer Ternary Blends for Photovoltaics. *Adv. Mater.* **2011**, *23*, 4093–4097.